Research Square

Preprints are preliminary reports that have not undergone peer review.
They should not be considered conclusive, used to inform clinical practice,
or referenced by the media as validated information.

Interfacial design and spin effects in room temperature magnetic photocatalysts for sustainable hydrogen production

R. Sagayaraj

sagayaraj@sjctnc.edu.in

St. Joseph's College of Arts and Science (Autonomous)

Systematic Review

Keywords: room-temperature magnets, spin polarization, photocatalytic hydrogen evolution, heterojunctions, chirality-induced spin selectivity, ferrites, sustainable energy

Posted Date: November 25th, 2026

DOI: https://doi.org/10.21203/rs.3.rs-11745354/v1

License: This work is licensed under a Creative Commons Attribution 4.0 International License.
Read Full License

Additional Declarations: No competing interests reported.

Interfacial design and spin effects in room temperature magnetic photocatalysts for sustainable hydrogen production

R. Sagayaraj

PG & Research Department of Physics, St. Joseph's College of Arts and Science (Autonomous), Cuddalore-607001, Affiliated to Annamalai University, Chidambaram, Tamil Nadu, India

Abstract

Photocatalytic water splitting is a promising route to sustainable hydrogen, but charge recombination and sluggish oxygen evolution still limit its efficiency. Adding a magnetic or spin degree of freedom to the catalyst is a growing strategy for addressing both. This review examines room-temperature magnetic ("quantum magnet") materials for hydrogen production, and covers four areas. First, we survey the materials: spinel ferrites, magnetic insulators and spin-polarized oxides, and above-room-temperature two-dimensional magnets such as Fe_3GaTe_2. Second, we analyze interface and heterojunction designs that couple a magnetic component to a light-absorbing semiconductor. Third, we compare the synergies between magnetism and photocatalysis, from Lorentz-force and spin-polarization effects to field-free chirality-induced spin selectivity. Fourth, we benchmark reported performance across ferrite photocatalysts, field-assisted systems, oxygen-evolution photo anodes and existing reviews. Magnetic-field gains are real but moderate, mostly in the 1.3–3× range. Across the few comparable studies the gain rises with field strength (1.33× at 108 mT, 1.5× at 140 mT, 2.97× at 500 mT), but the systems differ too much to separate field from material, and interface engineering alone often provides comparable gains. Two gaps are evident: few studies include controls that separate magnetic effects from thermal and mass-transport effects, and field-free spin routes and two-dimensional room-temperature magnets have not yet been shown to evolve hydrogen. We close with priorities for standardized reporting and for the design of scalable, low-field or field-free photocatalytic devices.

Keywords: room-temperature magnets; spin polarization; photocatalytic hydrogen evolution; heterojunctions; chirality-induced spin selectivity; ferrites; sustainable energy

Corresponding author: R. Sagayaraj (sagayaraj@sjctnc.edu.in)

1. Introduction

Hydrogen produced from sunlight and water is widely regarded as a clean energy carrier. Photocatalytic and photoelectrochemical water splitting offer a direct route to it. Their efficiency is still limited by rapid recombination of photogenerated electron–hole pairs and sluggish surface reactions, especially the oxygen evolution reaction (OER) [1,2]. Solar water splitting is generally pursued through photocatalytic (PC), photoelectrochemical (PEC) and photovoltaic-electrochemical (PV-EC) routes, and recent reviews stress that efficiency and scalability are the main barriers to industrial use [3–7]. Particulate photocatalyst systems are potentially simpler, cheaper and easier to scale than photoelectrode systems, although their solar-to-hydrogen efficiencies are currently lower [8,9]. A growing body of work addresses this by adding a magnetic or spin degree of freedom to the catalyst. Magnetic-field modulation has been reported to promote charge-carrier separation, extend carrier lifetimes through spin polarization, and improve surface reactions in photocatalytic systems [1]. Related reviews on magnetic-field-enhanced electrocatalysis reach similar conclusions for the hydrogen, oxygen and CO_2 reduction reactions [2]. Reviews of spin-modulated oxygen electrocatalysis explain why: oxygen intermediates are singlets while O_2 has a triplet ground state, so spin alignment can ease triplet O–O bond formation [10–13].

The experimental evidence now covers several material families. In ferromagnetic $FeCoSe_2$ photoanodes, an applied magnetic field lowered charge-transfer resistance and reduced electron–hole recombination, and the authors attributed the gain to spin polarization shifting the d-band center [14]. In two-dimensional polar MoSSe, strong spin–orbit coupling enabled spin-dependent charge separation under a low external field [15]. Magnetic insulators such as yttrium iron garnet (YIG) have also been used as photoanodes. There, spin-aligned holes accumulate in the hybridized O 2p/Fe 3d valence band and enhance water oxidation, which makes YIG a platform for spin-selective photocatalysis [16]. In particulate systems, a Au-supported Fe_3O_4/N-TiO_2 superparamagnetic photocatalyst reached a reported solar-to-hydrogen (STH) efficiency of 11.9 ± 0.5% through local magnetic-field effects, with contributions from both the Lorentz force and spin polarization [17]. Spin polarization has also been induced chemically, as in Pt/TiO_2, where spin-polarized Ti 3d and Pt 5d states near the Fermi level extend carrier lifetimes [18]. Taken together, these findings have prompted recent summaries of spin-polarization strategies for solar hydrogen production across oxides, sulfides, ferroelectrics and chiral molecules [19]. Chirality-induced spin

selectivity (CISS) offers an alternative, field-free source of spin polarization, and has been reviewed for electrocatalysis and, more recently, for chiral photocatalysts and electron-spin control in photocatalysis [20–22].

Several gaps remain. Studies typically rely on large or continuously applied external fields, while materials that retain spin order at room temperature without one are much less explored. Interface design, meaning how magnetic and semiconducting components are coupled, is rarely discussed systematically across material classes. The mechanistic roles of Lorentz force, spin selectivity and magnetothermal effects are often conflated [1,2,17].

Aim and scope. This review examines room-temperature magnetic ("quantum magnet") materials for sustainable hydrogen production. It covers their spin physics, interfacial and heterojunction design, and synergies with photocatalysis. It compares material classes and operating conditions, then identifies the open challenges for scalable, field-free or low-field devices.

2. Room-temperature magnetic materials for photocatalytic hydrogen

2.1 Spinel ferrites and substituted ferrites

Spinel ferrites (MFe_2O_4, e.g. $NiFe_2O_4$ and $CoFe_2O_4$) are iron-oxide-based spinels. Most are soft magnets, so they can be magnetized and demagnetized easily. This makes them magnetically recoverable photocatalysts, and their band gap can be tuned through the choice of the A^{2+} cation [23]. Ferrites also tend to be good at the oxygen evolution step [23]. More recent work shows how composition controls both magnetism and activity. Co^{2+}- and Zn^{2+}-substituted $CuFe_2O_4$ samples were all superparamagnetic. In photo-electrocatalytic tests, $Cu_{95}Zn_5Fe$ gave the highest hydrogen output (304.3 mmol g^{-1}) at 94% Faradaic efficiency, while $Cu_{75}Co_{25}Fe$ reached nearly 100% efficiency [24]. Other recent ferrite studies show similar sensitivity to composition. $CuO/CuFe_2S_xO_{4-x}$ produced 7.45 mmol g^{-1} h^{-1} of hydrogen with an apparent quantum efficiency (AQE) of 2.45%, five times that of pristine $CuFe_2O_4$ [25]. Sm-substituted Ni–Zn ferrites gave up to 24.99 mmol $gcat^{-1}$ over four hours [26]. A $ZnFe_2O_4$ co-catalyst improved H_2 production in a $CuO/ZnFe_2O_4$ p–n junction through better charge separation and light absorption [27]. Dual-function spinel ferrites also respond to piezoelectric stimulation: sonication plus light gave 484 μmol g^{-1} h^{-1}, against 232 and 288 μmol g^{-1} h^{-1} for sonication or light alone [28]. Reviews of spinel ferrites as main photocatalysts and co-catalysts point to heterojunction construction and synthesis control as the main routes to improvement [23,29].

2.2 Magnetic insulators and spin-polarized oxides

Magnetic exchange can also produce spin polarization without chirality or an applied field. In yttrium iron garnet (YIG) photoanodes, illumination accumulates spin-aligned holes in the hybridized O 2p/Fe 3d valence band, and this correlates with improved water-splitting efficiency [16]. Ferromagnetic $FeCoSe_2$ reached a maximum photocurrent of 3.98 mA cm^{-2} at 1.23 V under an applied field [14]. In particulate systems, Au-supported Fe_3O_4/N-TiO_2 reached the 11.9 ± 0.5% solar-to-hydrogen efficiency noted earlier [17].

2.3 Two-dimensional van der Waals magnets

Most intrinsic two-dimensional (2D) ferromagnets order below room temperature. Fe_3GaTe_2 is the notable exception, with a Curie temperature (T_C) of about 350–380 K and strong perpendicular magnetic anisotropy [30]. Epitaxial wafer-scale films have shown T_C up to 420 K, and one-unit-cell films reached 345 K [31]. Fe_3GaTe_2/graphene heterostructures reached up to 400 K [32]. In the sources reviewed here, these materials have been developed for spintronics, not tested as hydrogen-evolution photocatalysts, although layered topological magnetic materials (semiconducting ferromagnets) have been examined as hydrogen-evolution electrocatalysts at high current densities [33]. Broader surveys of 2D magnets are available [34,35]. They therefore represent an opportunity for interfacial design, and we present them as such in the outlook without implying demonstrated activity. Table 1 summarizes the materials discussed in this section and links magnetic character to the hydrogen-relevant result. Soft and superparamagnetic oxides carry the particle-scale hydrogen results, namely 11.9 ± 0.5% solar-to-hydrogen efficiency for Au/Fe_3O_4/N-TiO_2 [17] and 304.3 mmol g^{-1} at 94% Faradaic efficiency for $Cu_{95}Zn_5Fe$ [24]. Garnet and selenide photoanodes are instead judged by photocurrent (3.98 mA cm^{-2} at 1.23 V for $FeCoSe_2$ [14]), so their numbers cannot be compared directly with particulate hydrogen rates [16]. Fe_3GaTe_2 orders at 350–420 K [30–32], about 50–120 K above room temperature (calculated from the cited values), yet it has no hydrogen data: the material class with the strongest room-temperature magnetism has the weakest photocatalytic evidence. Section 5 returns to these parameters in Tables 4–8.

Table 1 Representative room-temperature magnetic materials relevant to hydrogen production (all figures as reported in the cited works) [14,16,17,23,24,30–32]

Ref.	Material	Magnetic character	Reported hydrogen-relevant result
[23]	Spinel ferrites ($NiFe_2O_4$, $CoFe_2O_4$)	Soft magnets; room-temperature magnetization	Magnetically recoverable; tunable band gap; good OER ability
[24]	Co/Zn-substituted $CuFe_2O_4$	Superparamagnetic	304.3 mmol g^{-1} H_2 ($Cu_{95}Zn_5Fe$); ~100% Faradaic efficiency ($Cu_{75}Co_{25}Fe$)
[16]	Yttrium iron garnet (YIG)	Magnetic insulator	Spin-aligned holes; enhanced water splitting
[14]	$FeCoSe_2$ photoanode	Ferromagnetic	3.98 mA cm^{-2} at 1.23 V under magnetic field
[17]	$Au/Fe_3O_4/N\text{-}TiO_2$	Superparamagnetic	STH efficiency 11.9 ± 0.5%
[30–32]	Fe_3GaTe_2 (bulk, films, graphene heterostructures)	2D ferromagnet, T_C ~350–420 K, strong perpendicular magnetic anisotropy	Spintronic data only in sources found; no hydrogen data

3. Interfacial and heterojunction design

3.1 Heterojunction architectures as the starting point

Interface design in $ZnIn_2S_4$-based photocatalysts is well organized. Heterostructures there fall into five categories by charge-transfer mechanism: conventional type-I/II, p–n, Z-scheme, S-scheme, and co-catalyst-deposited systems [36]. These frameworks apply equally to magnetic components. A non-magnetic reference helps show what a magnetic partner adds. A $ZnIn_2S_4$/Ni-MOL (nickel metal–organic layer) heterojunction reached 4.75 mmol g^{-1} h^{-1} under visible light, about 8 times pure $ZnIn_2S_4$. Directional electron transfer from $ZnIn_2S_4$ to the Ni-MOLs separated the charges, and the AQE reached 23.3% [37]. S-scheme heterojunctions are a central design. Reviews describe

their evolution from Z-scheme systems, the internal built-in electric field that preserves redox ability, and oxide-based and metal–organic framework (MOF)-based variants [38–41].

3.2 Adding a spin-responsive component to the junction

A magnetically responsive partner changes the picture. In a $ZnIn_2S_4$/Ni-MOF (nickel MOF) type-II heterojunction, Ni ions act as magnetic response centers. Under a 500 mT static field, the optimized sample reached 71.91 mmol g^{-1} h^{-1}, which is 2.97 times the rate under light alone. Pristine Ni-MOF was essentially inactive, and $ZnIn_2S_4$ showed minimal magnetic response. The authors attribute the gain to Ni^{2+}-driven spin polarization prolonging carrier lifetimes [42]. This should not be read as a head-to-head comparison with [37], since the materials, conditions and reaction systems differ. It does show that the magnetic partner and the junction act together.

3.3 Spin polarization at the interface and surface

Spin polarization can also be set up chemically. At Pt/TiO_2, spin-polarized Ti 3d and Pt 5d orbitals near the Fermi level extend carrier lifetimes, and a shifted d-band center facilitates oxygen desorption [18]. In $FeCoSe_2$, spin polarization gives a more favorable d-band center and lowers the Gibbs free energy of oxygen evolution under a field [14]. The same logic works without any field when the spin state is engineered chemically: in a NiFe-MOF co-catalyst on $BiVO_4$, Fe incorporation switches the Ni d_z^2 orbital from spin-down to spin-up through asymmetric Fe–O–Ni coupling and lifts the photocurrent to 6.0 mA cm^{-2} at 1.23 V [43]. At the particle scale, Fe_3O_4/N-TiO_2 uses local magnetic-field effects (Lorentz force plus spin polarization) [17]. Table 2 and Figure 1 summarize the strategies. Figure 1 shows the common pathway: absorption in the semiconductor, spin-filtered transfer across the interface and surface hydrogen evolution. Table 2 shows where each strategy acts on that pathway. The non-magnetic Ni-MOL junction acts only on charge separation (4.75 mmol g^{-1} h^{-1}, AQE 23.3% [37]). The magnetic-center junction adds spin polarization (2.97× under 500 mT [42]). The d-band-center and local-field strategies act at the surface and at particle scale (3.98 mA cm^{-2} [14]; STH 11.9% [17]). The first two rows are the closest pair for isolating what the magnetic component adds, but they differ in material and conditions, which is why Section 5 treats the comparison cautiously.

Table 2 Interfacial design strategies for magnetically assisted hydrogen production [14,17,18,37,42]

Ref.	Strategy	System	Reported mechanism	Reported result
[37]	Non-magnetic heterojunction (reference)	$ZnIn_2S_4$/Ni-MOLs	Directional electron transfer	4.75 mmol g^{-1} h^{-1}; AQE 23.3%
[42]	Magnetic-center type-II junction	$ZnIn_2S_4$/Ni-MOF, 500 mT	Ni^{2+} spin polarization; longer carrier lifetime	71.91 mmol g^{-1} h^{-1} (2.97× light only)
[18]	Chemical-bond-induced spin polarization	Pt/TiO_2	Spin-polarized Ti 3d/Pt 5d states; shifted d-band center	Overall water splitting (details not stated in source snippet)
[14]	Spin-tuned d-band center	$FeCoSe_2$ photoanode	Spin polarization; lower OER free energy	3.98 mA cm^{-2} at 1.23 V
[17]	Local magnetic field	Au/Fe_3O_4/N-TiO_2	Lorentz force + spin polarization	STH 11.9 ± 0.5%

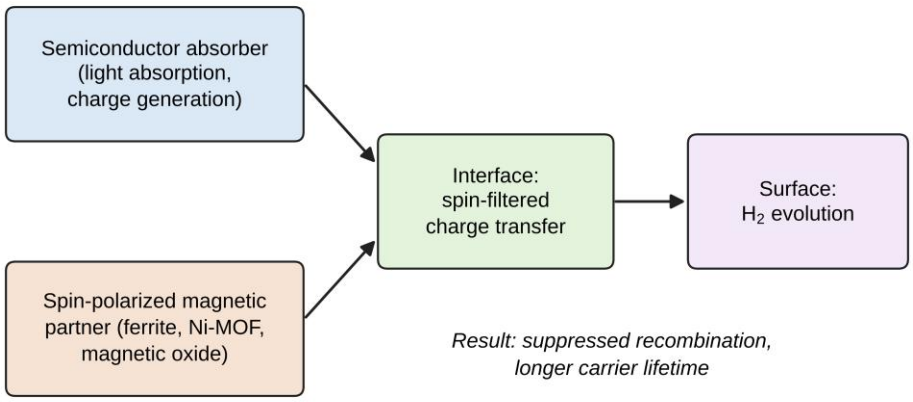


Fig. 1 Schematic of a magnetic/semiconductor interface: a light-absorbing semiconductor coupled to a spin-polarized magnetic partner, with spin-filtered charge transfer across the junction, suppressed recombination and hydrogen evolution at the surface [14,17,18,42]

4. Photocatalytic synergies

4.1 Field-assisted synergy: Lorentz force plus spin polarization

An external or local field acts on photocatalysis in more than one way at once. In Fe_3O_4/N-TiO_2, the Lorentz effect and spin polarization together prolonged exciton lifetime and gave the 11.9 ± 0.5% solar-to-hydrogen efficiency noted earlier [17]. Reviews of field-assisted photocatalysis similarly group the effects into negative magnetoresistance, Lorentz force and spin polarization, which influence light absorption, charge separation and surface reactions [1]. Keeping these contributions distinct is one of the open problems identified in the introduction. In Ag@g-C_3N_4 nanotubes, a magnetic field raised photocatalytic efficiency to a reported 200% above that of bulk g-C_3N_4 by lengthening carrier lifetimes under the Lorentz force [44]. For photoelectrodes, a $BiVO_4$/Fe_2TiO_5 photoanode showed that the field improves band alignment across the interface and promotes oxygen evolution at the Fe_2TiO_5/electrolyte interface, and the concept extends to TiO_2, WO_3 and Fe_2O_3 photoanodes [45]. A recent review covers the theory, spin detection and characterization methods for external-field photocatalysis [46]. In electrolysis, magnetic fields act largely on gas bubbles. Lorentz and Kelvin forces release paramagnetic O_2 bubbles at high current density, with the Lorentz contribution depending on field geometry and the Kelvin contribution on electrode magnetism [47]. A downward Lorentz force gave the smallest overpotentials for alkaline OER on Ni by disrupting the bubble layer and lowering mass-transfer resistance, while the intrinsic catalytic properties were unchanged [48]. A Lorentz-force-grown NiFe nano-cone array reached overpotentials of 199 mV at 10 mA cm^{-2} and 375 mV at 100 mA cm^{-2} [49]. Reviews separate the magnetohydrodynamic, spin-selection and magnetothermal contributions [50,51].

4.2 Field-free synergy: chirality-induced spin selectivity

Chirality-induced spin selectivity (CISS) offers spin polarization without an external field. In chiral ZnO, the chiral structure induces spin selectivity that extends photoexcited carrier lifetime by suppressing recombination and promotes spin-dependent reaction kinetics [52]. In chiral $(BiO)_2CO_3$, magnetic conductive atomic force microscopy (mc-AFM) shows the materials act as spin filters. Spin polarization rises with optical chirality, reaching 68.3% in the most strongly chiral sample. Photocurrent and oxygen-evolution kinetics improve, and H_2O_2 formation is suppressed [53]. Note that [53] studies oxygen evolution, not hydrogen evolution, so it supports the mechanism rather than a hydrogen yield. CISS and ferromagnetic order are complementary routes

to the same goal, which is spin-aligned charge carriers that favor triplet O_2 over peroxide. CISS has been reviewed for electrocatalysis (the oxygen evolution, oxygen reduction and hydrogen evolution reactions) [20], for chiral photocatalysts [22], and within broader electron-spin control strategies that also include defect engineering, magnetic-field regulation and metal coordination [21].

4.3 Practical synergy: magnetic recovery and heterojunction coupling

Magnetism also solves a practical problem for particulate photocatalysts, which is separating them from the suspension. Soft ferrites can be magnetized and demagnetized easily, which makes recovery straightforward [23]. Combining this with the heterojunction architectures of Section 3 [36,37] lets one material provide light absorption, a spin-responsive center and recoverability together [42]. Magnetic Fe_3O_4 cores make this concrete for hydrogen-evolving systems. Fe_3O_4@PPy@Pt/Ag@I (PPy, polypyrrole) combines a 6.2-fold higher hydrogen rate than its Pt-only analog with magnetic recovery and reuse [54], and recyclable Fe_3O_4@SiO_2/C_3N_5 gave higher H_2 production together with pollutant degradation [55]. Table 3 and Figure 2 summarize these synergies and separate them by whether an external field is needed. The field-assisted routes (rows 1 and 2) report the largest hydrogen numbers (STH 11.9% [17]; 71.91 mmol g^{-1} h^{-1} [42]) but need 180–500 mT. The field-free CISS routes (rows 3 and 4) remove the field, with spin polarization of 68.3% in chiral $(BiO)_2CO_3$ [53], but their evidence concerns carrier lifetime and oxygen evolution, not hydrogen yield [52,53]. Magnetic recovery (row 5) adds no photocatalytic gain but is independent of both field and mechanism [23]. Figure 2 shows the three routes converging on higher yield and durability, which Tables 4–8 test quantitatively.

Table 3 Synergy mechanisms linking magnetic order and photocatalysis [1,17,23,42,52,53]

Ref.	Synergy	External field?	Representative system	Reported outcome
[1,17]	Lorentz force + spin polarization	Yes (local or applied)	Fe_3O_4/N-TiO_2	STH 11.9 ± 0.5%
[42]	Spin polarization at a magnetic-center junction	Yes (500 mT)	$ZnIn_2S_4$/Ni-MOF	71.91 mmol g^{-1} h^{-1}; 2.97× light only

[52]	CISS (chiral spin selectivity)	No	Chiral ZnO	Longer carrier lifetime; spin-dependent kinetics
[53]	CISS, spin filtering	No	Chiral $(BiO)_2CO_3$	P = 68.3%; suppressed H_2O_2 (oxygen evolution study)
[23]	Magnetic recovery	No	Spinel ferrites	Easy magnetization and demagnetization

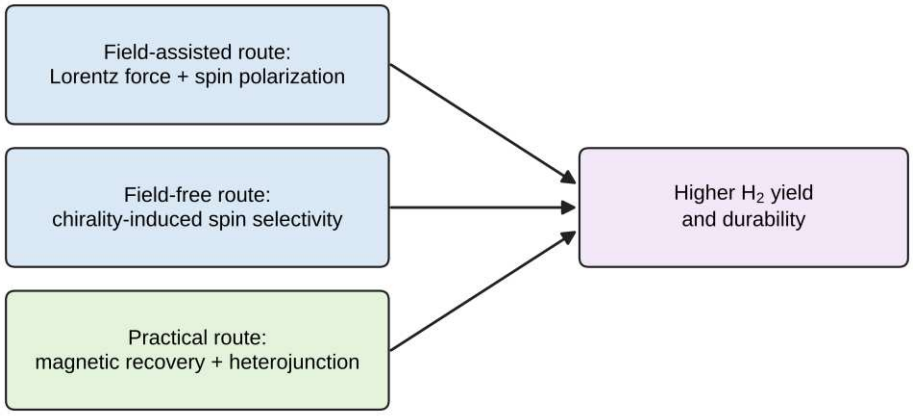


Fig. 2 Synergy map: field-assisted (Lorentz force plus spin polarization), field-free (CISS) and practical (magnetic recovery plus heterojunction) routes converge on higher H_2 yield and durability [1,17,23,42,52,53]

5. Results and discussion

5.1 Comparative performance of the reported systems

Figure 3 places four representative systems side by side. These values come from different papers with different lamps, sacrificial agents, loadings and field strengths, so the chart shows what was reported. It is not a ranking. The highest rate, 71.91 mmol g^{-1} h^{-1} for $ZnIn_2S_4$/Ni-MOF under 500 mT, is also the one with the clearest field effect (2.97× the light-only rate) [42]. Among field-assisted systems, an S-scheme hybrid reached 9.3 mmol g^{-1} h^{-1} at 108 mT. That is a 33% gain with an AQE of 13.2% at 420 nm, and density functional theory (DFT) calculations point to a spin-down Fe^{3+} 3d/O^{2-} 2p "spin highway" at the interface [56]. Heterojunctions without magnetic

components can also perform well. $CoFe_2O_4$/g-C_3N_4 p–n junctions reached 18.9 mmol g^{-1} h^{-1} through a built-in electric field alone [57].

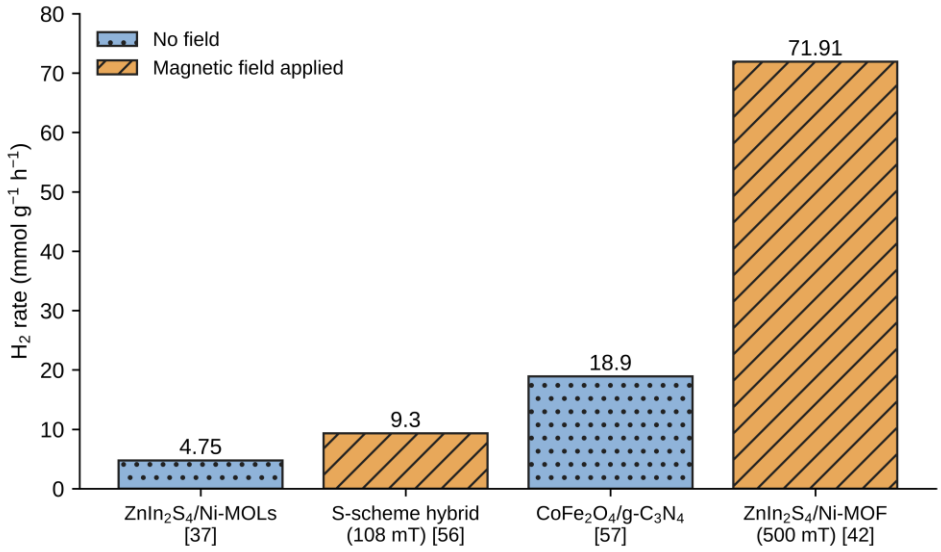


Fig. 3 Reported H_2 evolution rates for four representative systems [37,42,56,57]. Values are as reported; conditions are not normalized

Table 4 Benchmarking of reported magnetic-field effects on photocatalytic hydrogen evolution (as reported) [17,42,56–58]

Ref.	System	Field	Reported H_2 result	Field gain
[42]	$ZnIn_2S_4$/Ni-MOF	500 mT	71.91 mmol g^{-1} h^{-1}	2.97×
[56]	S-scheme heterojunction	108 mT	9.3 mmol g^{-1} h^{-1}; AQE 13.2%	+33%
[57]	$CoFe_2O_4$/g-C_3N_4	None	18.9 mmol g^{-1} h^{-1}	n/a (p–n junction only)
[58]	$CoOCu_2OZnO/TiO_2$/rGO	0.14 T	1,190 μmol g^{-1} vs 792 μmol g^{-1} over 4 h	~1.5×
[17]	Au/Fe_3O_4/N-TiO_2	180 mT (local field)	STH 11.9 ± 0.5%; 21.2 mmol g^{-1} h^{-1}; quantum efficiency 88.7% at 437 nm (reported at 270 °C)	not stated

5.2 What the comparison shows

Three patterns emerge. First, gains are real but moderate: field-assisted enhancements in Table 4 are mostly in the 1.3–3× range, and interface design often matters as much. For example, the non-magnetic $ZnIn_2S_4$/Ni-MOLs rate was about 8× that of the pristine semiconductor [37]. Second, weak controls limit interpretation. Reported gains combine Lorentz force, spin polarization and sometimes mass-transport or thermal effects [1,17], and few studies separate them with controls such as a non-magnetic analog under the same field. Third, field-free routes are less proven for hydrogen. CISS evidence so far is strongest for oxygen evolution and photocurrent [52,53], and Fe_3GaTe_2-type 2D magnets have spintronic but not photocatalytic data [30–32].

5.3 Priorities for the field

The most useful next steps are standardized reporting of field strength, lamp, scavenger and AQE; paired field-on/field-off and magnetic/non-magnetic controls; and testing of room-temperature 2D magnets and chiral spin filters as hydrogen photocatalysts.

5.4 Ferrite-based systems

Table 5 and Figure 4 collect recent ferrite studies [25–28,57]. They give a different picture from the field-assisted systems in Table 4. $CoFe_2O_4$/g-C_3N_4 reaches 18.9 mmol g^{-1} h^{-1} [57], well above the sulfur-doped copper ferrite junction (7.45 mmol g^{-1} h^{-1}) [25] and the Sm-substituted Ni–Zn ferrite, whose four-hour yield of 24.99 mmol $gcat^{-1}$ corresponds to roughly 6.2 mmol g^{-1} h^{-1} if the rate were constant (calculated from the cited values) [26]. The piezo-photocatalytic ferrite is lower in absolute rate (0.484 mmol g^{-1} h^{-1}) but is the only entry where a second stimulus produces a measured synergy, since light plus sonication exceeds either alone [28]. The key point is that none of these ferrite studies applies a magnetic field. Ferrites are used as semiconductors or co-catalysts, so their magnetism is a property they carry rather than a variable that was tested [23,29]. Magnetic cores add recovery: Fe_3O_4@PPy@Pt/Ag@I raised the hydrogen rate 6.2-fold over its Pt-only analog while remaining recoverable [54], and Fe_3O_4@SiO_2/Co–Cr–B kept more than 90% of its activity over six cycles in $NaBH_4$ hydrolysis, a chemical rather than photocatalytic reaction [59].

Table 5 Recent ferrite- and magnetite-based catalysts for hydrogen evolution (as reported) [25–28,54,57,59]

Ref.	System	Reported H_2 result	Design feature and condition
[25]	$CuO/CuFe_2S_xO_{4-x}$	7.45 mmol g^{-1} h^{-1}; AQE 2.45%	Sulfur doping plus CuO; 5× pristine $CuFe_2O_4$
[26]	Sm-substituted Ni–Zn ferrite	24.99 mmol $gcat^{-1}$ in 4 h (≈6.2 mmol g^{-1} h^{-1} average)	Composition tuning; photo/electrocatalytic
[57]	$CoFe_2O_4/g\text{-}C_3N_4$	18.9 mmol g^{-1} h^{-1}	p–n junction with built-in electric field
[28]	Dual-function metal ferrite	484 μmol g^{-1} h^{-1} (vs 232 and 288 alone)	Piezo-photocatalysis: sonication plus light
[27]	$CuO/ZnFe_2O_4$ (Prussian-blue-analog-derived)	Higher H_2 rate than bare CuO	$ZnFe_2O_4$ as co-catalyst in p–n junction
[54]	Fe_3O_4@PPy@Pt/Ag@I	6.2× the H_2 rate of Fe_3O_4@PPy@Pt	Polyiodide-boosted transport; magnetic recovery
[59]	$Fe_3O_4@SiO_2$/Co–Cr–B ($NaBH_4$ hydrolysis)	>90% activity after six cycles	Magnetic recovery; chemical hydrolysis, not photocatalysis

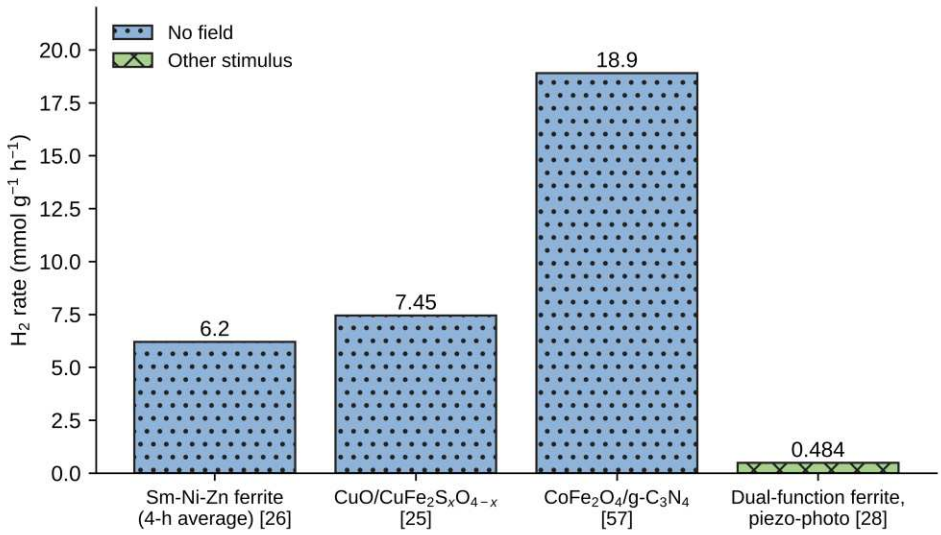


Fig. 4 Reported hydrogen rates of ferrite-based systems [25,26,28,57]. The Sm–Ni–Zn value is our four-hour average. No magnetic field was applied in these studies, and conditions are not normalized

5.5 Correlating field strength and gain

Figure 5 plots reported gain against applied field for the three studies where both are stated. Gain rises from 1.33× at 108 mT [56] to 1.5× at 140 mT [58] and 2.97× at 500 mT [42]. A monotonic trend is suggested, but three points from three different materials, light sources and reaction systems cannot separate the effect of field from the effect of material. The Au/Fe_3O_4/N-TiO_2 system, at 180 mT, sits in this field range but reports its benefit as a solar-to-hydrogen efficiency (11.9 ± 0.5%) instead of a gain [17], so it cannot be placed on the plot. A dose–response study within a single material, with the field varied at fixed light, would settle the question.

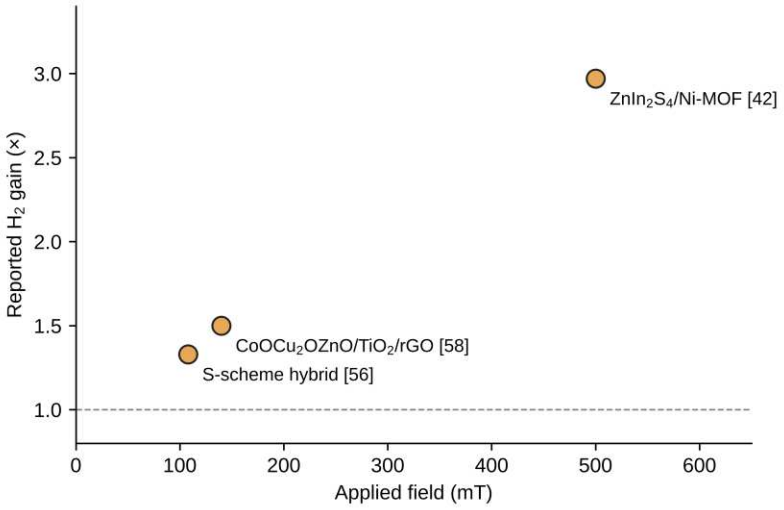


Fig. 5 Reported hydrogen gain versus applied magnetic field for three systems [42,56,58]. Dashed line: no gain

5.6 Where this review sits among existing reviews

Table 6 groups the reviews retrieved in this survey. Each covers part of the topic: field-assisted photocatalysis [1,46], spin and magnetic effects in oxygen electrocatalysis [2,10–13], CISS and chiral catalysts [20,22], general electron-spin control [21], ferrite photocatalysts [23,29] and S-scheme design [38–41]. Among those retrieved, none treats room-temperature magnetic materials, their interfaces and hydrogen production together. That is the scope of the present review.

Table 6 Existing reviews retrieved and the gap this review addresses [1–7,10–13,20–23,29,38–41,46]

Theme	**Reviews**	**What they leave open**
Solar H_2 routes (PC, PEC, PV-EC)	[3–7]	Role of spin and magnetism
Field-assisted photocatalysis	[1,46]	Room-temperature magnets as materials
Spin and magnetism in oxygen electrocatalysis	[2,10–13]	Photocatalytic hydrogen evolution
CISS and chiral catalysts	[20,22]	Combination with ferromagnetic order
Electron-spin control in photocatalysis	[21]	Interface design across magnet classes
Ferrite photocatalysts	[23,29]	Magnetism as a tested variable

S-scheme heterojunctions	[38–41]	Spin-responsive components in the junction

5.7 Oxygen-evolution and photoanode evidence

Table 7 and Figure 6 collect recent studies of magnetic and spin effects on the oxygen-evolution half-reaction, which limits both electrolysis and photoelectrochemical water splitting. Three observations emerge. First, in electrolysis the benefit is largely hydrodynamic: a downward Lorentz force gave the smallest overpotentials on Ni without changing the intrinsic catalytic properties [48], and a Lorentz-force-grown NiFe nano-cone array reached 199 mV at 10 mA cm^{-2} and 375 mV at 100 mA cm^{-2} [49]. Second, on photoanodes the gains come from combining a spin-active or magnetic partner with a junction: NiFe-MOF/$BiVO_4$ delivers 6.0 mA cm^{-2} at 1.23 V versus the reversible hydrogen electrode (RHE) [43], and $BiVO_4$/FeCoMOF delivers 6.2 mA cm^{-2}, 3.8 times bare $BiVO_4$ [60], which implies about 1.6 mA cm^{-2} for the bare electrode (calculated from the cited values). The ferromagnetic $FeCoSe_2$ photoanode under field gave 3.98 mA cm^{-2} [14]. Third, the field can also act during synthesis: hematite grown under 1 T gave a 74% higher photocurrent and a 33 mV photovoltage gain through magnetically induced texturing and densification [61]. Figure 6 compares the photocurrents. Electrolytes and illumination differ between studies, so the figure shows reported values and not a ranking.

Table 7 Magnetic and spin effects on oxygen evolution and photoanodes [14,43,45,47–49,60,61]

Ref.	System	Mechanism	Reported result
[48]	Ni wire, alkaline OER	Downward Lorentz force disrupts the bubble layer	Smallest overpotential among field directions tested; catalytic properties unchanged
[47]	γ-Fe_2O_3-coated electrodes	Lorentz and Kelvin forces on O_2 bubbles	Dominant contribution at high current density
[49]	NiFe nano-cone arrays (Lorentz-force-assisted growth)	Field during deposition; improved bubble release	199 mV at 10 mA cm^{-2}; 375 mV at 100 mA cm^{-2}

[45]	$BiVO_4/Fe_2TiO_5$ photoanode	Field improves spin polarization and band alignment	Concept extended to TiO_2, WO_3 and Fe_2O_3 photoanodes
[43]	NiFe-MOF/$BiVO_4$	Spin-state transition of Ni d_z^2 through Fe–O–Ni coupling	6.0 mA cm^{-2} at 1.23 V vs RHE
[60]	$BiVO_4$/FeCoMOF p–n junction	Type-II junction separates carriers	6.2 mA cm^{-2} at 1.23 V vs RHE; 3.8× bare $BiVO_4$
[61]	Hematite grown under 1 T	Magnetically induced texturing and densification	Photocurrent +74%; photovoltage +33 mV

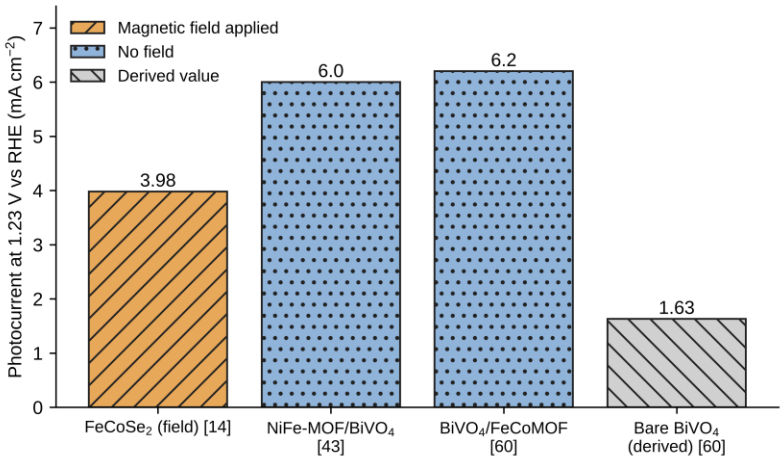


Fig. 6 Reported photocurrent densities at 1.23 V vs RHE for photoanodes with a magnetic or spin-engineered component [14,43,60]. The bare-$BiVO_4$ bar is derived from the reported 3.8-fold gain

5.8 Correlating parameters across the tables and figures

Table 8 collects the parameters that recur across Tables 1–7 and Figures 3–6 and correlates them. Values marked derived are calculated here from the cited numbers. Three conclusions follow. First, field strength and gain rise together (Figure 5), yet the field-off baselines differ by about 5× between the magnetic $ZnIn_2S_4$/Ni-MOF junction and its non-magnetic Ni-MOL counterpart, so material and junction design contribute at least as much as the field [37,42]. Second, field-free ferrite junctions reach 0.8–2.0× the rate of the field-assisted S-scheme system (Table 5 against

Table 4) [25,56,57], and a second non-magnetic stimulus, sonication, gives a gain of about 1.7× [28], within the range of the magnetic gains (1.33–2.97×) [42,56,58]. Third, the parameters that would link magnetism directly to activity, namely ordering temperature, spin polarization and field strength, are rarely reported together with hydrogen yield. Fe_3GaTe_2 has the first without the last [30–32], chiral $(BiO)_2CO_3$ has the second for oxygen evolution only [53], and a field-on/field-off comparison is reported in only three of the studies compared here [42,56,58]. Closing that gap is the aim of the roadmap in Section 6.

Table 8 Parameters recurring across the tables and figures, correlated [14,16,17,25,28,30–32,37,42,43,53,56–58,60]

Parameter	**Where it appears**	**Reported values**	**Interpretation**
Applied field vs gain	Tables 2–4; Figure 5	108 mT: 1.33× [56]; 140 mT: 1.5× [58]; 500 mT: 2.97× [42]	Gain rises with field, but material and conditions differ
Field-on vs field-off baseline	Table 4; Figure 3	71.91 mmol g^{-1} h^{-1} at 500 mT [42], about 24.2 without field (derived); 4.75 for the non-magnetic Ni-MOL junction [37]	Field-off baseline is about 5× the non-magnetic reference, larger than the 2.97× field effect
Field-assisted vs field-free rate	Tables 4–5; Figures 3–4	9.3 mmol g^{-1} h^{-1} at 108 mT [56]; 7.45 and 18.9 with no field [25,57]	Field-free junctions reach 0.8–2.0× the field-assisted rate (derived)
Second-stimulus synergy	Table 5; Figure 4	484 μmol g^{-1} h^{-1} for light plus sonication vs 288 and 232 alone [28]; about 1.7× the best single stimulus (derived)	Same order as the magnetic gains of 1.33–2.97×
Quantum efficiency	Tables 2 and 4	AQE 23.3% [37]; 13.2% at 420 nm [56]; 2.45% [25]; quantum efficiency 88.7% at 437 nm and 270 °C [17]	Wavelength, temperature and reaction system differ, so values are not comparable

Ordering temperature vs 300 K	Table 1	Fe_3GaTe_2: 350–380 K [30]; up to 420 K in films [31]; up to 400 K in graphene heterostructures [32]	About 50–120 K above room temperature (derived); no hydrogen data
Spin polarization	Table 3	P = 68.3% in chiral $(BiO)_2CO_3$ [53]; spin-aligned holes in YIG [16]	Oxygen-evolution and photocurrent evidence; hydrogen yield not yet linked to P
Photocurrent at 1.23 V	Table 7; Figure 6	3.98 mA cm^{-2} for $FeCoSe_2$ under field [14]; 6.0 for NiFe-MOF/$BiVO_4$ [43]; 6.2 for $BiVO_4$/FeCoMOF, 3.8× its bare $BiVO_4$ (about 1.6, derived) [60]	Spin- or junction-engineered $BiVO_4$ exceeds the field-assisted $FeCoSe_2$ value; electrolytes and light differ

6. Challenges and outlook

Table 9 and Figure 7 turn the gaps identified above into a research agenda. The first two rows (separating field effects and non-comparable benchmarks) follow from the spread of conditions in Table 4 [17,42,56–58]. The next two (field-free hydrogen and untested 2D magnets) follow from the oxygen-evolution-only CISS evidence and the spintronic-only Fe_3GaTe_2 data [30–32,52,53]. The last combines recovery with junction design [23,36,42].

Table 9 Open challenges and proposed research directions [1,17,23,30–32,36,42,52,53,56–58]

Challenge	**Evidence from this review**	**Proposed direction**
Separating field effects	Lorentz, spin and mass-transport effects often reported together [1,17]	Paired field-on/off and magnetic/non-magnetic controls
Non-comparable benchmarks	Different lamps, scavengers and field strengths (Table 4) [42,56–58]	Standard protocol with AQE and STH reporting
Field-free hydrogen	CISS evidence is mostly for oxygen evolution [52,53]	Test chiral spin filters in full H_2-evolving systems
Untested 2D magnets	Fe_3GaTe_2 has spintronic data only [30–32]	Build Fe_3GaTe_2 heterojunctions with semiconductors

Scalability and recovery	Magnetic recovery works for ferrites [23]	Combine recovery with heterojunction design [36,37,42]

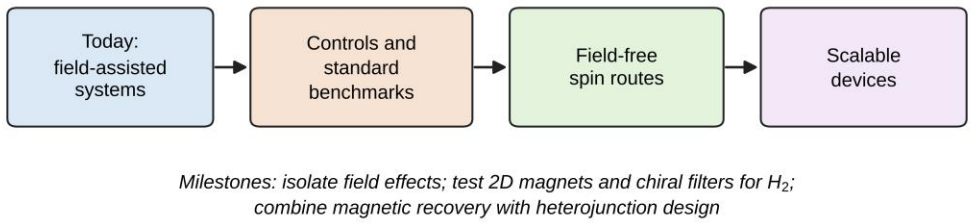


Fig. 7 Roadmap from today's field-assisted systems, through controls and standard benchmarks and field-free spin routes, to scalable devices [1,23,30–32,52,53]

7. Conclusion

Room-temperature magnetic materials offer several routes to better photocatalytic hydrogen production, and the reported data allow them to be compared. Ferrites and magnetic oxides deliver the strongest particle-scale results: Au/Fe_3O_4/N-TiO_2 reached a solar-to-hydrogen efficiency of 11.9 ± 0.5%, Co/Zn-substituted $CuFe_2O_4$ produced up to 304.3 mmol g^{-1} of hydrogen at 94% Faradaic efficiency, and $CoFe_2O_4$/g-C_3N_4 reached 18.9 mmol g^{-1} h^{-1} without any applied field. Magnetically responsive heterojunctions add spin control to light absorption: $ZnIn_2S_4$/Ni-MOF reached 71.91 mmol g^{-1} h^{-1} under 500 mT, which is 2.97 times its light-only rate. For the oxygen-evolution half-reaction, a Lorentz-force-grown NiFe array reached 199 mV at 10 mA cm^{-2}, and spin- or junction-engineered $BiVO_4$ photoanodes reached 6.0–6.2 mA cm^{-2} at 1.23 V, against 3.98 mA cm^{-2} for field-assisted $FeCoSe_2$.

The correlated data show that the gains are moderate and not yet separable from material effects. Gain rose from 1.33× at 108 mT to 1.5× at 140 mT and 2.97× at 500 mT, but the light-only baseline of the magnetic junction (about 24.2 mmol g^{-1} h^{-1}) was already about five times the rate of its non-magnetic counterpart (4.75 mmol g^{-1} h^{-1}). Field-free ferrite junctions reached 0.8–2.0 times the rate of the field-assisted S-scheme system (9.3 mmol g^{-1} h^{-1} at 108 mT), and a second non-magnetic stimulus, sonication, gave a gain of about 1.7×, within the range of the magnetic gains.

Field-free spin routes are promising, with spin polarization of 68.3% in chiral $(BiO)_2CO_3$, but this evidence concerns carrier lifetime and oxygen evolution, not hydrogen yield. Fe_3GaTe_2 orders at 350–420 K, about 50–120 K above room temperature, yet has no hydrogen data. The priorities are therefore paired field-on and field-off controls, standardized reporting of field, light and quantum efficiency, and tests of above-room-temperature two-dimensional magnets and chiral spin filters as hydrogen photocatalysts.

Declarations

Funding: The authors received no specific funding for this work.

Data availability: Not applicable.

Clinical trial number: Not applicable.

Ethics approval and consent to participate: Not applicable.

Consent for publication: Not applicable.

Competing interests: The authors declare no competing interests.

Third-party material: Not applicable.

References

1. Li R, Qiu L-P, Cao S-Z, Li Z, Gao S-L, Zhang J, Ramakrishna S, Long Y-Z. Research advances in magnetic field-assisted photocatalysis. Adv Funct Mater. 2024. https://doi.org/10.1002/adfm.202316725
2. Belgami MA, Patra A, Jeong SM, Rout CS. Exploring the synergy of magnetism and electrocatalysis: a comprehensive review on mechanisms, recent developments and future perspectives. J Mater Chem A. 2024;12:24005–24040. https://doi.org/10.1039/d4ta02468k
3. Zheng Y, Ma M, Shao H. Recent advances in efficient and scalable solar hydrogen production through water splitting. Carbon Neutrality. 2023;2(1):1–15. https://doi.org/10.1007/s43979-023-00064-6
4. Martens JA. The bright future of solar-driven hydrogen production. Front Sci. 2024;2:1532051. https://doi.org/10.3389/fsci.2024.1532051
5. Imran S, Hussain M. Emerging trends in water splitting innovations for solar hydrogen production: analysis, comparison, and economical insights. Int J Hydrogen Energy. 2024;77:975–996.

6. Recent progress in hydrogen: from solar to solar cell. J Mater Sci Technol. 2024. https://doi.org/10.1016/j.jmst.2023.08.030 [authors and volume to add]
7. Elevating the prospects of green hydrogen (H_2) production through solar-powered water splitting devices: a systematic review. Sustain Mater Technol. 2024. https://doi.org/10.1016/j.susmat.2024.e00972 [authors to add]
8. Hisatomi T, Wang Q, Zhang F, Ardo S, Reisner E, Nishiyama H, Kudo A, Yamada T, Domen K. Photocatalytic water splitting for large-scale solar-to-chemical energy conversion and storage. Front Sci. 2024;2:1411644. https://doi.org/10.3389/fsci.2024.1411644
9. Nandy S, Hisatomi T, Takata T, Setoyama T, Domen K. Recent advances in photocatalyst sheet development and challenges for cost-effective solar hydrogen production. J Mater Chem A. 2023;11:20470–20479. https://doi.org/10.1039/D3TA04353C
10. Taspya T, Snigdha RY, Islam M, Islam MM. Advances in spin-modulated electrocatalysis of oxygen evolution reaction. ChemistrySelect. 2024. https://doi.org/10.1002/slct.202401073
11. Fang Z, Zhao W, Shen T, Qiu D, Lv Y, Hou X, Hou Y. Spin-modulated oxygen electrocatalysis. Precis Chem. 2023. https://doi.org/10.1021/prechem.3c00059
12. Advances in spin catalysts for oxygen evolution and reduction reactions. Small. 2023;19(5):e2205638. [authors to add]
13. Spin-selective catalysts for oxygen-involved electrocatalysis. Adv Energy Sustain Res. 2025;6(5):2400326. [authors to add]
14. Fan B, Yu Z, Ding L, Jiang R, Hou Y, Li S, Chen J. Magnetic field enhancement of the $FeCoSe_2$ photoanode for the oxygen evolution reaction. Catal Sci Technol. 2023;13:4451–4465. https://doi.org/10.1039/D3CY00633F [title to confirm]
15. Roy K, Ghosh D, Maitra S, Kumar P. Enhanced hydrogen evolution reaction via photoelectrochemical water splitting utilizing asymmetric MoSSe under a low external magnetic field. J Mater Chem A. 2023;11:21135–21145. https://doi.org/10.1039/D3TA03227B
16. Gajapathy H, Bandaranayake S, Hruska E, Vadakkayil A, et al. Spin polarized electron dynamics enhance water splitting efficiency by yttrium iron garnet photoanodes. Chem Sci. 2024. https://doi.org/10.1039/D3SC03016D [authors, volume and pages to confirm]
17. Local magnetic spin mismatch promoting photocatalytic overall water splitting with exceptional solar-to-hydrogen efficiency. Energy Environ Sci. 2022.

https://doi.org/10.1039/D1EE02222A [authors to add; the 180 mT, 21.2 mmol g^{-1} h^{-1} and 270 °C values in Table 4 come from the accepted-manuscript version, please confirm]

18. Liao L, Li Z, Lu J, Xu Y, Zhou W, Wu Y. Chemical bond induced spin polarization towards optimized photocatalytic overall water splitting. Appl Catal B. 2025. [journal details to confirm]
19. Progress in manipulating spin polarization for solar hydrogen production. Mater Rep Energy. 2024;4(1):1–15. [authors to add]
20. Chae K, Mohamad NARC, Kim J, Won D-I, Lin Z, Kim J, Kim DH. The promise of chiral electrocatalysis for efficient and sustainable energy conversion and storage: a comprehensive review of the CISS effect and future directions. Chem Soc Rev. 2024;53:9029–9058. https://doi.org/10.1039/D3CS00316G
21. Fang J, Liu Y, Lin Z, et al. Optimizing photocatalysis via electron spin control. Chem Soc Rev. 2025;54:2154–2187. https://doi.org/10.1039/D4CS00317A
22. Harnessing chirality in nanomaterials: advancing photocatalysis for hydrogen production and beyond. EES Catal. 2026;4:502–521. https://doi.org/10.1039/D5EY00314H [authors to add]
23. Ma H, Liu C. A mini-review of ferrites-based photocatalyst on application of hydrogen production. Front Energy. 2021;15(3):621–630. https://doi.org/10.1007/s11708-021-0761-0
24. Cantoni M, et al. Partially substituted magnetic ferrites as Pt-free catalysts for hydrogen evolution from water photo-electrolysis. 2026. [journal and DOI to confirm]
25. Hussain E, Jalil M, Abid MZ, Mansab J, Althomali RH, Wang S, Rauf A, Rafiq K. Insights into the development and performance of $CuO/CuFe_2S_xO_{4-x}$ catalysts: an effective approach for renewable hydrogen generation. Mater Adv. 2024;5:6572–6585. https://doi.org/10.1039/D3MA01137B
26. High performance Sm-substituted Ni-Zn catalysts for green hydrogen generation via photo-electro-catalytic water splitting processes. J King Saud Univ Sci. 2024;36:103426. https://doi.org/10.1016/j.jksus.2024.103426 [authors to add]
27. Prussian blue analogues-derived $ZnFe_2O_4$ in $CuO/ZnFe_2O_4$ p–n junction for H_2 production. ACS Omega. 2024;9(43):43734–43742. https://doi.org/10.1021/acsomega.4c06231 [authors to add]
28. Jabeen S, Saleem M, Mumtaz F, Javed S, Ali M, Khan MZ, Koh J-H, Maqbool A, Baluch AH, Niazi MBK, Hussain I. Coupling the power of spinel nanoparticles: dual-function metal

ferrite catalysts for advanced piezo-photocatalytic and electrocatalytic water splitting. J Mater Chem A. 2025. https://doi.org/10.1039/D5TA01180A

29. Mohammed Y, Hafeez HY, Mohammed J, Suleiman AB, et al. Hydrogen production via photocatalytic water splitting using spinel ferrite-based photocatalysts: recent and future perspectives. Next Energy. 2024.
30. Zhang G, Guo F, Wu H, Wen X, Yang L, Jin W, Zhang W, Chang H. Above-room-temperature strong intrinsic ferromagnetism in 2D van der Waals Fe_3GaTe_2 with large perpendicular magnetic anisotropy. Nat Commun. 2022;13:5067. https://doi.org/10.1038/s41467-022-32605-5
31. Wu S, He Z, Gu M, et al. Robust ferromagnetism in wafer-scale Fe_3GaTe_2 above room-temperature. Nat Commun. 2024;15. https://doi.org/10.1038/s41467-024-54936-1 [volume/article number to confirm]
32. Shinwari T, Khan KIA, Lv H, et al. Above-room-temperature ferromagnetism in large-area epitaxial Fe_3GaTe_2/graphene van der Waals heterostructures. arXiv:2505.06128 [preprint; replace with journal version if available]
33. Gupta S, Świątek H, Sawczak M, Klimczuk T, Bogdanowicz R. Investigating layered topological magnetic materials as efficient electrocatalysts for the hydrogen evolution reaction under high current densities. Catalysts. 2024;14(10):676.
34. Papavasileiou AV, Menelaou M, Sarkar KJ, Sofer Z, Polavarapu L, Mourdikoudis S. Ferromagnetic elements in two-dimensional materials: 2D magnets and beyond. Adv Funct Mater. 2023.
35. The magnetic genome of two-dimensional van der Waals materials. ACS Nano. 2022;16(5):6960–7079. https://doi.org/10.1021/acsnano.1c09150 [authors to add]
36. Liu C, Zhang Q, Zou Z. Recent advances in designing $ZnIn_2S_4$-based heterostructured photocatalysts for hydrogen evolution. J Mater Sci Technol. [year, volume and pages to confirm]
37. Li Y, Huang Y, Zhang H, Wang X, Gao L, Zhang Y, Liao Y, Meng J, Cui Y, Dai W-L. In-situ construction of 3D/2D $ZnIn_2S_4$/Ni-MOLs: highly efficient visible-light-driven photocatalytic heterojunction in hydrogen evolution. Appl Catal B Environ Energy. 2025. https://doi.org/10.1016/j.apcatb.2024.124657

38. Dharani S, Vadivel S, Gnanasekaran L, Rajendran S. S-scheme heterojunction photocatalysts for hydrogen production: current progress and future prospects. Fuel. 2023;349:128688. https://doi.org/10.1016/j.fuel.2023.128688
39. Ullah I, Amin M, Zhao P, Qin N, Xu A-W. Recent advances in inorganic oxide semiconductor-based S-scheme heterojunctions for photocatalytic hydrogen evolution. Inorg Chem Front. 2025;12:1329–1348. https://doi.org/10.1039/D4QI02797C
40. Kumar A, Khosla A, Sharma SK, Dhiman P, Sharma G, Gnanasekaran L, Naushad M, Stadler FJ. A review on S-scheme and dual S-scheme heterojunctions for photocatalytic hydrogen evolution, water detoxification and CO_2 reduction. Fuel. 2023;333:126267. https://doi.org/10.1016/j.fuel.2022.126267
41. Yuan L, Du P, Yin L, Yao J, Wang J, Liu C. Metal–organic framework-based S-scheme heterojunction photocatalysts. Nanoscale. 2024. https://doi.org/10.1039/D3NR06677K
42. $ZnIn_2S_4$/Ni-MOF ferromagnetic heterojunction photocatalyst under a static magnetic field (photo-magnetic catalytic hydrogen evolution). [authors, journal and year to confirm]
43. Asymmetric coupling induces spin-flipping in the NiFe-MOF cocatalyst for boosting the $BiVO_4$ photoanode water oxidation. J Mater Chem A. 2026. https://doi.org/10.1039/D6TA03699F [authors to add]
44. Enhanced photocatalytic activity of Ag@g-C_3N_4 nanotubes by regulating photogenerated carriers to bypass the recombination center under the Lorentz force. Phys Chem Chem Phys. 2023;25:16371–16379. https://doi.org/10.1039/D3CP01455J [authors to add]
45. Enhancing photoelectrochemical water oxidation using ferromagnetic materials and magnetic fields. J Am Chem Soc. 2024. https://doi.org/10.1021/jacs.4c13017 [authors and volume to add]
46. Liu P, Mao X. Photocatalytic performance enhancement using external magnetic fields: a review. Adv Mater Interfaces. 2025.
47. Li X, Hao C, Du Y, Lu Y, Fan Y, Wang M, Wang N, Meng R, Wang X, Xu ZJ, Cheng Z. Harnessing magnetic fields to accelerate oxygen evolution reaction. Chin J Catal. 2023. https://doi.org/10.1016/S1872-2067(23)64560-7 [volume and pages to add]
48. Fogaça W, Ikeda H, Misumi R, Kuroda Y, Mitsushima S. Enhancement of oxygen evolution reaction in alkaline water electrolysis by Lorentz forces generated by an external magnetic field. Int J Hydrogen Energy. 2024. https://doi.org/10.1016/j.ijhydene.2024.02.199

49. Liu H, Jia Y, Hua S, Weng J, Wang L, Yang C. Lorentz force-assisted growth of romanesco-like Ni–Fe nano-cone arrays for enhanced oxygen evolution reaction at high current densities. Nanoscale. 2025;17:8466–8475. https://doi.org/10.1039/D4NR05174B
50. Hu H, Lu J, Sun L, Xu F, Huang P, Peng H, Zou Y, Chu H, Zhang H. Magnetic enhancement effect and research progress in oxygen evolution reaction. 2023. https://doi.org/10.1360/TB-2022-1133 [journal to confirm]
51. Magnetic field effects on electrocatalysis (Lorentz-force visualization of ion motion in OER and ORR). Nat Commun. 2024. https://doi.org/10.1038/s41467-024-46980-8 [authors and exact title to confirm]
52. Chiral ZnO photocatalyst with chirality-induced spin selectivity. Nat Commun. 2023. https://doi.org/10.1038/s41467-023-40367-x [authors and exact title to confirm]
53. Shi Y, Sun Z, Wang Y, Fu X, Song Z, Xie Z, Lin H. Chiral $(BiO)_2CO_3$ catalysts with spin-selective charge transport enhance photocatalytic oxygen evolution. Nanoscale. 2026. https://doi.org/10.1039/D6NR00364H
54. Zhang W, Jiang C, Tao W, Wang Y, Guan H, Hao L. Enhanced photocatalytic hydrogen evolution by polyiodide-boosted electron transport and Pt–Ag alloy active sites in conductive polymer-based core–shell photocatalysts. RSC Sustain. 2026;4(3). https://doi.org/10.1039/D5SU00533G
55. Yang J, Gao Y, Li X, Wang Y, Guan P, Liu B. Recyclable magnetic Fe_3O_4@SiO_2/C_3N_5 photocatalyst with enhanced H_2 production and organic pollutant degradation performance. Mater Sci Semicond Process. 2024. https://doi.org/10.1016/j.mssp.2024.108267
56. A field-programmable S-scheme heterojunction enabled by spin-polarized electron highway for solar hydrogen generation. Chem Eng J. 2026;527. [authors to add]
57. He W, Liu L, Ma T, Han H, Zhu J, Liu Y, Fang Z, Yang Z, Guo K. Controllable morphology $CoFe_2O_4$/g-C_3N_4 p-n heterojunction photocatalysts with built-in electric field enhance photocatalytic performance. Appl Catal B Environ. 2022;306.
58. Areerob Y, Meng Z, Ullah K, Wijaya K, Otgonbayar Z, Oh W-C. Magnetic and ultrasonic integrated photocatalytic hydrogen evolution effects with nanosize $CoOCu_2OZnO$ and TiO_2 decorated on reduced graphene oxide. 2023. [journal, volume and pages to confirm]

59. Lakhali H, Şahin Ö, Ceyhan AA. A novel core–shell Fe_3O_4@SiO_2/Co–Cr–B magnetic catalyst for efficient and reusable hydrogen evolution from $NaBH_4$ hydrolysis. New J Chem. 2025;49:11304–11325. https://doi.org/10.1039/D5NJ01445J

60. Chen Q, He Y, Ge J, Zhang J, Wang D, Tian C, Wu A, Fu H. Construction of type-II $BiVO_4$/FeCoMOF p–n heterojunction for enhanced photoelectrochemical water oxidation. Nano Res. 2026;19:94908454. https://doi.org/10.26599/NR.2026.94908454

61. Pires [initials to add], et al., Mathur S. Field-directed growth of hematite for advanced solar hydrogen production. Adv Energy Sustain Res. 2026;7(1):e202500313. https://doi.org/10.1002/aesr.202500313 [author list to complete]